Redox cycling of iridium(III) complexes gives versatile materials for photonics applications

Collin D. Morris,[a] Mariana Spulber,[b] Markus Neuburger,[a] Cornelia G. Palivan,[b] Edwin C. Constable,*[a] and Catherine E. Housecroft*[a]

[a]Department of Chemistry, University of Basel, Spitalstrasse 51, CH-4056, Basel, Switzerland.

[b]Department of Chemistry, University of Basel, Klingelbergstrasse 80, CH-4056, Basel, Switzerland.

Email: catherine.housecroft@unibas.ch

Abstract

The cyclometallated iridium(III) complex $[Me_4N][Ir(ppy)_2(cat)]$ (Hppy = 2-phenylpyridine; H_2cat = benzene-1,2-diol) has been prepared under inert atmosphere and structurally characterized by single crystal X-ray diffraction. Under ambient conditions, the fully reduced complex (as formulated) undergoes rapid one-electron oxidation both in solution and in the solid state to a species containing a semiquinone ligand. The resultant neutral complex $[Ir(ppy)_2(sq)]$ (sq = *o*-semiquinone) was also prepared by exposing the reaction mixture to O_2 during the course of the reaction. Electron paramagnetic resonance (EPR) spectroscopy confirms the diamagnetic nature of the complex $[Me_4N][Ir(ppy)_2(cat)]$ and indicates that the unpaired electron in $[Ir(ppy)_2(sq)]$ resides primarily on the sq ligand. The photophysical, electrochemical, and spectroelectrochemical properties of $[Ir(ppy)_2(sq)]$ were investigated and reveal the changes in absorption as the complex is converted into the catecholate and quinone forms.

Keywords: iridium; semiquinone; spectroelectrochemistry; X-ray structure

1. Introduction

Cyclometallated iridium(III) complexes are the focus of research for technologies such as light-emitting electrochemical cells (LECs) and organic light-emitting diodes (OLEDs) due to their high photoluminescence quantum yields and the relative ease of tuning their emission wavelengths via functionalization of the ligands.[1–8] Neutral compounds are required for OLEDs, whereas cationic $[Ir(C^N)_2(N^N)]^+$ complexes with a neutral bidentate donor and two cyclometallated ligands are the commonest materials utilized in LECs.[1,2,8] Metal-binding domains within the C^N and N^N ligands include 2-phenylpyridine, 2-phenylpyrazole,[9] 2-thienylpyridine,[10] 2,2′:6′,2″-terpyridine,[11,12] 1,10-phenanthroline,[13] imidazole,[14] and triazole;[15] systematic variation allows tuning of the HOMO and LUMO energies and the related emission properties and device performances. However, the core structure remains cationic with the attendant materials properties (solubility in polar solvents, presence of an anion) which influence processability and device assembly and performance. Anionic iridium(III) complexes have been less studied but compounds $[Ir(C^N)_2X_2]^-$ (X = CN^-,[16–18] NCS^-,[19] NCO^- [20]) have shown promise in LECs. Complexes with 'hard base', benzene-1,2-diolate ligands (Scheme 1) have been reported, [21] with compounds containing TCC^{2-} or TBC^{2-} being stable in ambient conditions and exhibiting emissions at 600 and 590 nm, respectively. In contrast, complexes derived from H_2DTBC can only be isolated only in the paramagnetic, semiquinone form.[22]

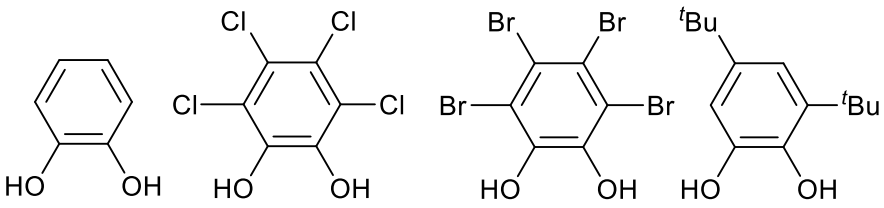

H_2cat H_2TCC H_2TBC H_2DTBC

Scheme 1. Structures of benzene-1,2-diol (H_2cat), 3,4,5,6-tetrachlorobenzene-1,2-diol (H_2TCC), 3,4,5,6-tetrabromobenzene-1,2-diol (H_2TBC), and 3,5-di-*tert*-butylbenzene-1,2-diol (H_2DTBC).

Our interests lie in the development of modular strategies for the design and systematic investigation of materials for OLEDs (neutral) and LECS (charged) as well as a long term goal of achieving single component white-light emitters. The benzene-1,2-diolate compounds attracted our attention as a series which allow access to anionic, neutral and cationic complexes by cycling through the oxidation states of the non-innocent ligand (Scheme 2).

The stability of the anionic $[Ir(ppy)_2(TCC)]^-$ and $[Ir(ppy)_2(TBC)]^-$ complexes is attributed to the strong electron-withdrawing groups on the benzene-1,2-diolate ligands.[23] Since the redox potentials of H_2cat lie between those of H_2DTBC and H_2TCC, it was unclear whether complexes would favor the diolate, semiquinonate, or quinone oxidation level under ambient conditions.

We report the synthesis of the new anionic complex $[Ir(ppy)_2(cat)]^-$ under inert conditions along with its characterization by single crystal X-ray diffraction. This material was unstable towards oxidation, resulting in isolation of the neutral semiquinonate complex $[Ir(ppy)_2(sq)]$ (sq = *o*-semiquinone) in the bulk phase. The paramagnetic nature was confirmed by EPR spectroscopy and detailed studies of the photophysical, electrochemical, and spectroelectrochemical properties are reported.

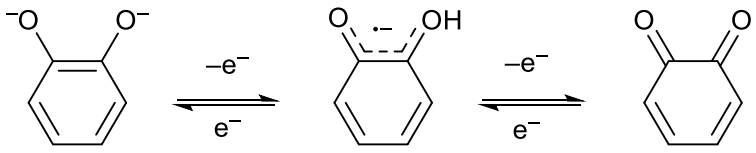

benzene-1,2-diolate semiquinonate quinone

Scheme 2. Different oxidation states of benzene-1,2-diolate.

2. Experimental

2.1 Materials

Hydrated iridium(III) chloride (Johnson Matthey), 2-phenylpyridine (Aldrich), and tetramethylammonium hydroxide (Fluka) were used without further purification. Benzene-1,2-diol was purchased from Fluka and was recrystallized from toluene before use. $[Ir_2(ppy)_4Cl_2]$ was prepared according to the standard literature method.[24] Silica gel (silica gel 60, 0.040-0.063 mm) was purchased from Fluka.

2.2 General

^{1}H NMR spectra were recorded using a Bruker Avance III-500 NMR spectrometer at 295 K. Chemical shifts were referenced to residual solvent peaks with δ(TMS) = 0 ppm. ESI-MS and MALDI-TOF spectra were recorded on Bruker Esquire 3000plus and Microflex Bruker Daltonics instruments, respectively. Solution absorption and emission spectra were recorded on a Varian-Cary 5000 spectrophotometer and Shimadzu RF-5301 PC spectrofluorometer, respectively, in HPLC grade dichloromethane. IR spectra were recorded from 4000-400 cm^{-1} using a Perkin Elmer Spectrum Two UATR spectrometer. Electrochemical measurements were performed using a CH Instruments 900B potentiostat with glassy carbon, platinum wire, and silver wire as the working, counter, and reference electrodes, respectively. Cyclic voltammograms were recorded on samples dissolved in degassed HPLC grade acetonitrile (~10^{-4} mol·dm^{-3}) with [^{n}Bu_4N][PF_6] (~0.1 mol·dm^{-3}) as the supporting electrolyte. Experiments were run with a scan rate of 0.1 V s^{-1} and internally referenced to Fc/Fc^+. Spectroelectrochemical measurements were performed on CH_2Cl_2 solutions (~10^{-3} mol dm^{-3}) at room temperature with [^{n}Bu_4N][PF_6] (~0.1 mol dm^{-3}) as the supporting electrolyte. The solution was added to an optically transparent thin-layer electrochemical (OTTLE) cell with two Pt minigrid electrodes (working and auxiliary), a silver wire pseudoreference electrode, and a path length of ~0.2 mm. The potential was controlled using a

VersaSTAT 3 potentiostat from Princeton Applied Research. Electron paramagnetic resonance (EPR) spectra were recorded on a Bruker CW EPR Elexsys-500 spectrometer equipped with a variable temperature unit. Measurements were performed at 297 K and 100 K with the following parameters: microwave power 2 mW, number of scans up to 30, modulation amplitude 5 G, and sweep width 400 G for room temperature spectra and 1000 G for low temperature spectra. Simulations were performed using the Bruker SimFonia simulation package. For spectra resulting from a superposition of contributions of paramagnetic species, the fit determined the relative intensity of each component with a typical error of 10%.

2.3 Synthesis of $[Me_4N][Ir(ppy)_2(cat)]$

$[Ir_2(ppy)_4Cl_2]$ (100 mg, 0.0933 mmol, 1.0 equiv.), benzene-1,2-diol (20.6 mg, 0.187 mmol, 2.01 equiv.), and tetramethylammonium hydroxide pentahydrate (37.4 mg, 0.187 mmol, 2.01 equiv.) were dissolved in 10 mL anhydrous MeOH under N_2. The yellowish solution was heated to reflux and turned red after ~30 mins. The reaction mixture was allowed to reflux under N_2 for 16 h, cooled to room temperature, and filtered under an inert atmosphere into a Schlenk tube using a Schlenk filter. Samples for EPR measurements were removed from this solution and transferred quickly to the sample container. X-ray quality single crystals were grown over several days by layering diethyl ether over the methanol reaction mixture under nitrogen.

2.4 Synthesis of $[Ir(ppy)_2(sq)]$

$[Ir_2(ppy)_4Cl_2]$ (100 mg, 0.0933 mmol, 1.0 equiv.), catechol (20.6 mg, 0.187 mmol, 2.01 equiv.), and tetramethylammonium hydroxide pentahydrate (37.4 mg, 0.187 mmol, 2.01 equiv.) were dissolved in 10 mL MeOH. The yellowish solution was first stirred under nitrogen for 30 min then bubbled with air for ~1 h at room temperature, over which time it began to turn green in color. The reaction was then refluxed

for 16 h, cooled to room temperature, filtered and the solvent removed under reduced pressure. The crude product was purified using flash column chromatography (silica, CH_2Cl_2 changing to 100:2 CH_2Cl_2:MeOH as eluent) resulting in a dark green solid (90 mg, 80% yield). ^{1}H NMR (500 MHz, CD_3CN, 295 K) δ/ppm 8.88 (bd, J = 2 Hz, 2H), 7.86 (d, J = 8 Hz, 2H), 7.65 (m, 4H), 7.22 (bd, J = 4 Hz, 2H), 6.72 (t, J = 8 Hz, 2H), 6.61 (t, J = 8 Hz, 2H), 6.13 (bd, J = 6 Hz, 2H). ESI-MS m/z: 501.0 $[M–sq]^+$ (calc. 501.1). MALDI-TOF MS m/z: 501.1 $[M–sq]^+$ (calc. 501.1). IR (solid, $\tilde{\nu}$ / cm^{-1}): 3055 (w), 3031 (w), 2952 (m), 2920 (m), 2853 (m), 1606 (m), 1580 (m), 1561 (w), 1515(m), 1477 (s), 1464 (m), 1452 (m), 1438 (m), 1415 (s), 1366 (m), 1346 (w), 1314 (w), 1305 (m), 1267 (m), 1254 (m), 1244 (m), 1225 (m), 1156 (m), 1123 (w), 1112 (w), 1105 (w), 1060 (m), 1029 (m), 1007 (m), 882 (w), 792 (w), 753 (s), 736 (s), 726 (s), 669 (m), 653 (w), 630 (m), 606 (m), 559 (m), 509 (w), 497 (w), 477 (w), 417 (m). UV-Vis (CH_2Cl_2, 3.00 × 10^{-5} mol dm^{-3}) λ/nm (ε/dm^3 mol^{-1} cm^{-1}): 261 (35 900), 297 (19 100), 351 (5 790), 403 (3 360), 451 (2 550). Suitable elemental analysis could not be obtained.

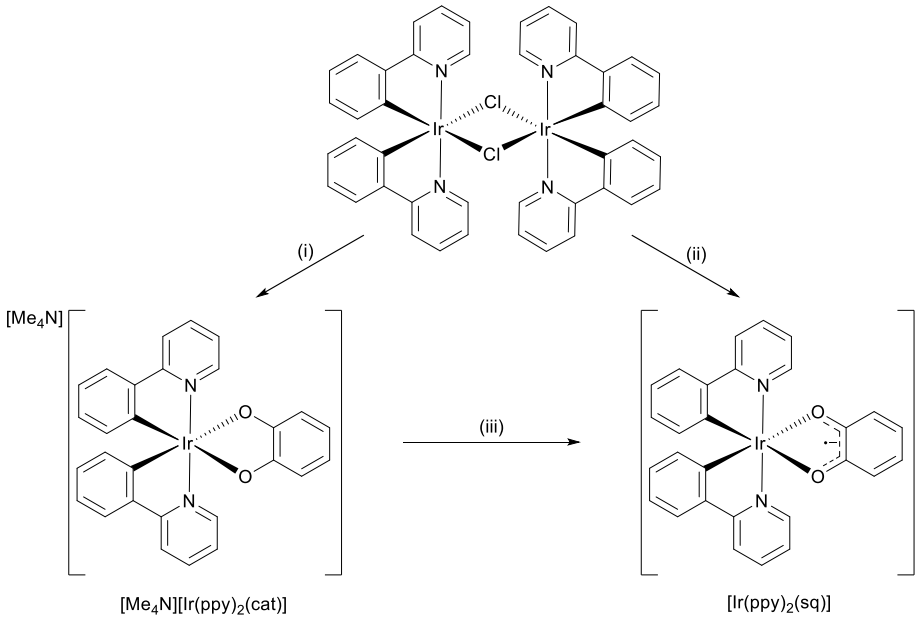

Scheme 3. Synthesis of anionic benzene-1,2-diolate and neutral semiquinonate iridium(III) complexes. Conditions: (i) benzene-1,2-diol, $[Me_4N]OH$, MeOH, 65 °C, N_2, 16 h; (ii) benzene-1,2-diol, $[Me_4N]OH$, bubbling air, MeOH, 65 °C, 16 h; (iii) exposure to O_2.

2.5 X-ray Crystallography

Intensity data were collected on a Bruker APEX-II diffractometer with data reduction, solution, and refinement using the APEX2,[25] SIR92,[26] and SHELX-13[27] programs, respectively. Structural analysis was carried out using Mercury v. 3.6.[28,29]

2.6 Single crystal X-ray determination of $[Me_4N][Ir(ppy)_2(cat)]\cdot 2CH_3OH\cdot H_2O$

$C_{68}H_{82}Ir_2N_6O_9$, M = 1511.87, red block, orthorhombic, space group *Iba*2, a = 17.8126(16), b = 18.3727(16), c = 18.9496(17) Å, U = 6201.6(10) Å^3, Z = 4, D_c = 1.619 Mg m^{-3}, μ(Cu-Kα) = 8.691 mm^{-1}, T = 123 K. Total 33906 reflections, 5503 unique, R_{int} = 0.036. Refinement of 5436 reflections (387 parameters) with $I > 2\sigma(I)$ converged at final R_1 = 0.0193 (R_1 all data = 0.0195), wR_2 = 0.0210 (wR_2 all data = 0.0212), gof = 1.0945.

3. Results and Discussion

3.1 Synthesis of iridium complexes and NMR transparency

The reduced, anionic form of the iridium dioxolene complex was prepared by the reaction of the chlorido-bridged dimer $[Ir_2(ppy)_4Cl_2]$ with a slight excess of benzene-1,2-diol and $[Me_4N]OH$ as base in methanol under a nitrogen atmosphere (Scheme 3). The reaction mixture changed color from yellow to red within minutes of heating and remained red under an inert atmosphere. After refluxing overnight and during workup this complex was found to be very unstable and could not be isolated as a bulk phase. The product quickly changes color from red to green upon exposure to aerial oxygen in solution or the solid state, resulting in formation of the neutral semiquinone complex $[Ir(ppy)_2(sq)]$.

A second synthesis was performed in which air was bubbled through the reaction mixture for 1 hour after stirring under nitrogen for 30 minutes. Exposure to O_2 again caused the color of the reaction mixture to turn from red to green during this time, indicative of the formation of the semiquinone. After heating to reflux overnight, the solvent was removed and the crude product purified by flash column chromatography (~80% yield).

The ^{1}H NMR spectrum of [Ir(ppy)$_2$(sq)] in CD_3CN only shows signals assigned to the cyclometallated ligands of the complex (Fig. 1). The lack of signals for the semiquinone ligand is consistent with the localization of the unpaired electron on the semiquinone domain. Only the $[Ir(ppy)_2]^+$ fragment was observed in either ESI-MS or MALDI-TOF MS, and we therefore turned to EPR spectroscopy for additional characterization of the complex (see later).

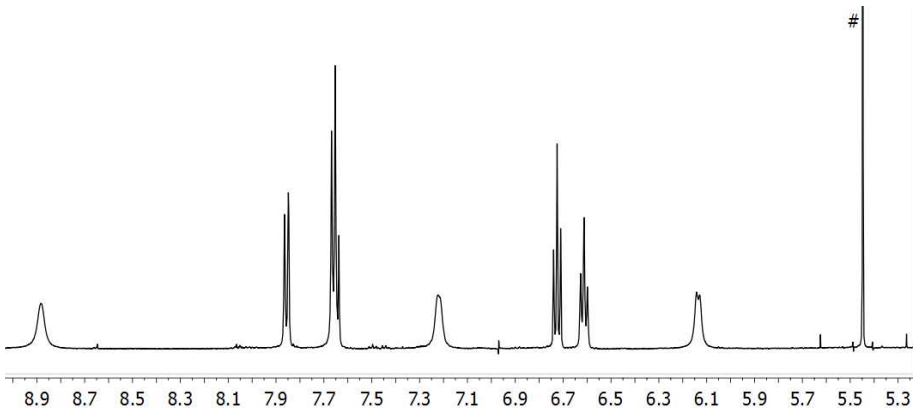

Fig. 1 Aromatic region of 500 MHz 1H NMR spectrum of [Ir(ppy)$_2$(sq)] (295 K, CD_3CN). Chemical shifts in δ/ppm. # = residual CH_2Cl_2.

3.2 Single crystal structure of anionic complex

Single crystals of $[Me_4N][Ir(ppy)_2(cat)]\cdot 2CH_3OH\cdot H_2O$ were grown under an inert atmosphere by layering diethyl ether over the methanol reaction mixture after Schlenk filtration. Red crystals of this reduced form of the complex were quickly taken from solution, placed in oil, and mounted in order to prevent oxidation to the semiquinone form. The complex crystallizes in the polar orthorhombic space group *Iba*2 with both

enantiomers of the octahedral iridium anion in the unit cell. Two methanol molecules and a single water co-crystallize along with the metal complex and $[Me_4N]^+$ cation to make up the asymmetric unit. All atoms lie on general positions except for O5 of the water molecule, which resides on Wyckoff position 4b with site symmetry ..2; its second hydrogen atom is therefore symmetry generated. The N-donors of the cyclometallated $[ppy]^-$ ligands are *trans* to one another and the complex exhibits typical bond lengths and angles between the iridium center and coordinated ligands (Fig. 2). More significant are the C-O bond lengths of 1.349(4) Å (C1-O1) and 1.347(3) Å (C6-O2) in the chelated benzene-1,2-diolate ligand. These bond lengths are consistent with those found in other benzene-1,2-diolate complexes and are significantly longer than those found in the semiquinone form of $[Ir(2\text{-}(p\text{-tolylpyridine}))_2(DTBsq)]$ (DTBsq = 3,5-di-*tert*-butyl-*o*-semiquinone) (1.295(5) and 1.291(5) Å).[22] The C1-C6 bond length of 1.416(4) Å and all other C-C bonds within the benzene-1,2-diolate ligand (1.383(5)-1.402(4) Å) provide further support for the aromatic character of the ligand. The extended structure lacks any π-stacking interactions; however, edge-to-face π-interactions between the pyridine H3 and centroid of the catecholate ligand form a one-dimensional chain along the [010] direction (Fig. 3a). The chain comprises complexes of alternating handedness (Fig. 3b) generated by a glide plane with $CH_{py}\cdots\pi_{cat}$ distances of 2.59 Å (H to centroid). Both chelating oxygen atoms of the benzene-1,2-diolate ligand are also involved in hydrogen bonding interactions with nearby methanol molecules with distances of 1.79 Å and 1.84 Å for O1···H1 and O2···H2, respectively. Several hydrogens of the tetramethylammonium cation are also involved in CH···π interactions with phenyl and benzene-1,2-diolate arene rings with distances ranging from 2.75-2.89 Å (H to centroid).

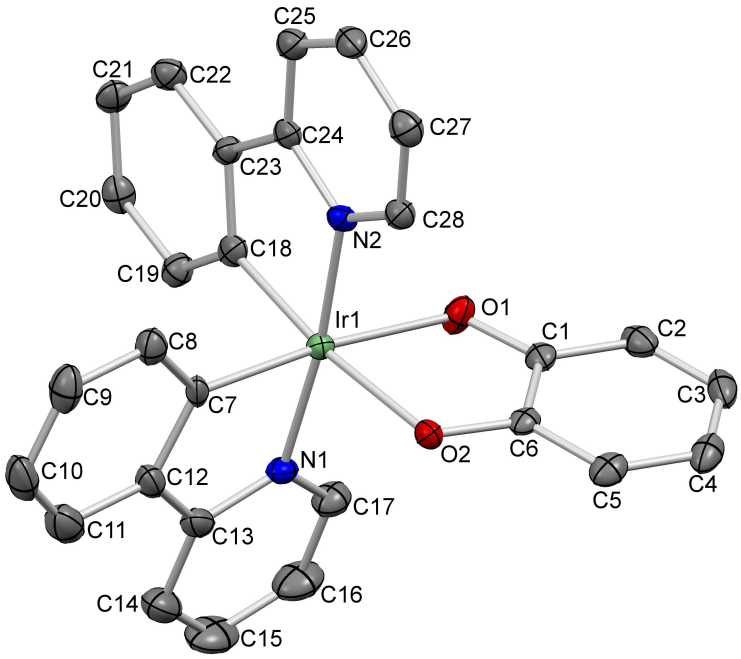

Fig. 2 Structure of the Λ-[Ir(ppy)2(cat)]- anion in $[Me_4N][Ir(ppy)_2(cat)]\cdot 2CH_3OH\cdot H_2O$ (H atoms omitted for clarity, 50% ellipsoid probability). Selected bond lengths (Å) and angles (°): C1-O1 = 1.349(4), C6-O2 = 1.347(3), Ir1-O1 = 2.135(2), Ir1-O2 = 2.145(2), Ir1-N1 = 2.027(2), Ir1-N2 = 2.024(2), Ir1-C7 = 1.997(3), Ir1-C18 = 1.990(2); O1-Ir1-O2 = 78.47(8), N1-Ir1-C7 = 80.9(1), N2-Ir1-C18 = 81.0(1), O1-Ir1-C7 = 173.6(1), O2-Ir1-C18 = 172.9(1), N1-Ir1-N2 = 173.64(9).

(a)

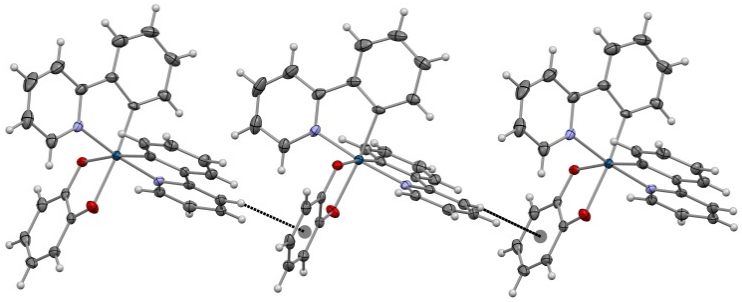

(b)

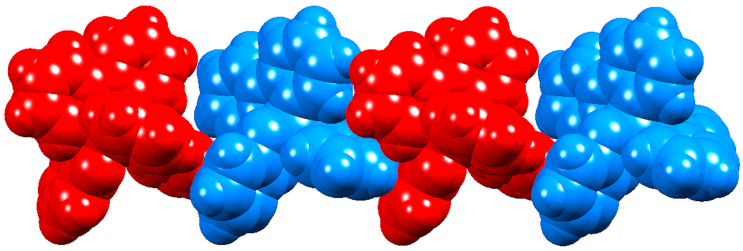

Fig. 3 (a) One-dimensional chain running along the b-axis formed by short edge-to-face interactions between the pyridine H3 and centroid of the benzene-1,2-diolate ligand (dotted line, 2.59 Å). (b) Alternating Δ- and Λ-enantiomers running along each chain.

3.3 EPR spectroscopy

Electronic paramagnetic resonance (EPR) spectra were recorded for the benzene-1,2-diolate and semiquinone forms of the iridium complexes at 297 and 100 K. An aliquot of the reaction mixture for the anionic complex was removed and quickly added to the sample holder. As expected, no signal was detected at room temperature for this diamagnetic complex (Fig. 4, blue trace). The EPR spectrum of the purified semiquinone complex showed a single sharp signal with a g value of 1.986, similar to that reported for the semiquinone form of [Ir(2-(p-tolylpyridine))$_2$(DTBsq)] (g = 1.987) and other iridium-dioxolene complexes, proving the coordination of the semiquinone radical as a radical anion to the iridium(III) center (Fig. 4, black trace) [22],[30].

The low temperature EPR spectrum of Ir(ppy)$_2$(sq) displays rhombic symmetry with g_x = 2.037, g_y = 1.98 and g_z = 1.93 (Fig. 5a). Surprisingly, when the sample of [Me$_4$N][Ir(ppy)$_2$(cat)] was cooled to 100 K for low temperature EPR measurement, the red solution turned immediately to green. The EPR spectrum of this sample at low temperature also suggests a complex with rhombic symmetry but appears to contain two species in a ~3:1 ratio (Fig. 5b). The g_x, g_y, and g_z values of the major and minor components were calculated as 2.038, 1.97, and 1.93 and 2.14, 1.98, and 1.92, respectively. The characteristic and small variation in the anisotropic g values indicate that there is limited mixing of the

ligand p and metal d orbitals, with the former having a much greater contribution. Therefore, it is clear the unpaired electron is localized mainly on the *o*-semiquinone ligand, as was also reported for [Ir(2-(p-tolylpyridine))$_2$(DTBsq)].[22]

Upon warming to room temperature, the sample remains green and the measured EPR spectrum is similar to that of the oxidized semiquinone complex with g = 1.98 (Fig. 4, red trace). This suggests that cooling the anionic form of the complex causes its irreversible oxidation to the semiquinone form and is most likely driven by the condensation of O_2.

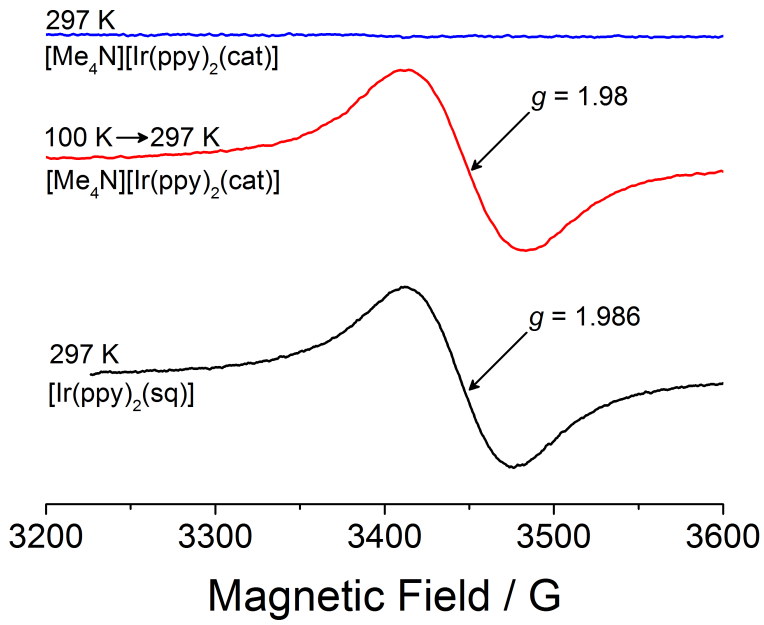

Fig. 4 EPR spectra of [Me$_4$N][Ir(ppy)$_2$(cat)] at room temperature (blue trace) and room temperature after being cooled to 100 K (red trace). EPR spectrum of [Ir(ppy)$_2$(sq)] at room temperature (black trace).

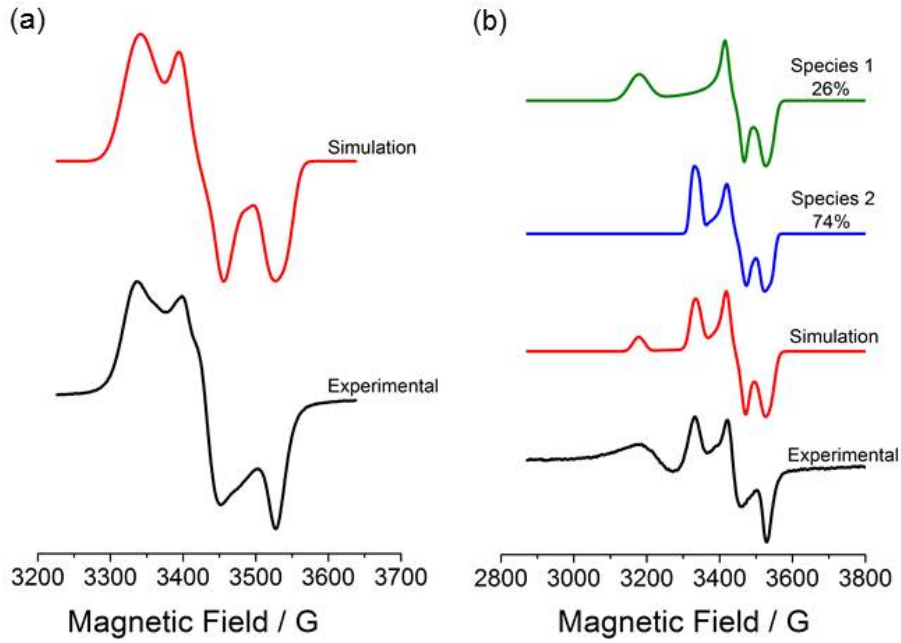

Fig. 5 (a) Simulated (red trace) and experimental (black trace) EPR spectra of [Ir(ppy)$_2$(sq)] at 100 K. (b) Simulated (green, blue, and red traces) and experimental (black trace) EPR spectra of [Me$_4$N][Ir(ppy)$_2$(cat)] at 100 K.

3.4 Photophysical properties

The solution absorption spectrum of [Ir(ppy)$_2$(sq)] in CH_2Cl_2 is dominated by intense bands in the UV region, with λ_{max} at 261 nm (Fig. 6). These arise from ligand-centered $\pi^* \leftarrow \pi$ transitions and extend to ~325 nm. The absorptions observed at wavelengths above 350 nm have extinction coefficients (ε) that are more than an order of magnitude less than those at higher energy, and are assigned to metal-to-ligand charge transfer (MLCT) transitions. The absorption spectra of [Ir(ppy)$_2$(sq)] and [Ir(2-(p-tolylpyridine))$_2$(DTBsq)] [22] have many similar features although the latter has well-defined MLCT absorption around 600 nm; when comparing the two complexes, only a slight difference in the most intense absorption and its corresponding extinction coefficient is observed (261 nm and 35,900 dm^3 mol^{-1} cm^{-1} *versus* 267 nm and 36,700 dm^3 mol^{-1} cm^{-1}, respectively).

Very weak photoluminescence was observed in CH_2Cl_2 solutions of [Ir(ppy)$_2$(sq)] at room temperature upon excitation into either the ligand-centered or MLCT absorption bands. This agrees well with the lack of luminescence observed for [Ir(2-(p-tolylpyridine))$_2$(DTBsq)] [22]. Unfortunately, solutions of [Me_4N][Ir(ppy)$_2$(cat)] were too unstable towards oxidation to investigate their photophysical properties in detail.

The FTIR spectrum of [Ir(ppy)$_2$(sq)] contains bands indicative of a bis(cyclometallated) Ir(III) complex. However, the relatively intense band at 1438 cm^{-1} is most notable, as it is assigned to the C–O stretching mode of the metal-bound *o*-semiquinone, and agrees well with the band observed at 1440 cm^{-1} in [Co(trien)(DTBsq)]Cl_2 (trien = 1,8-diamino-3,6-diazaoctane) [31].

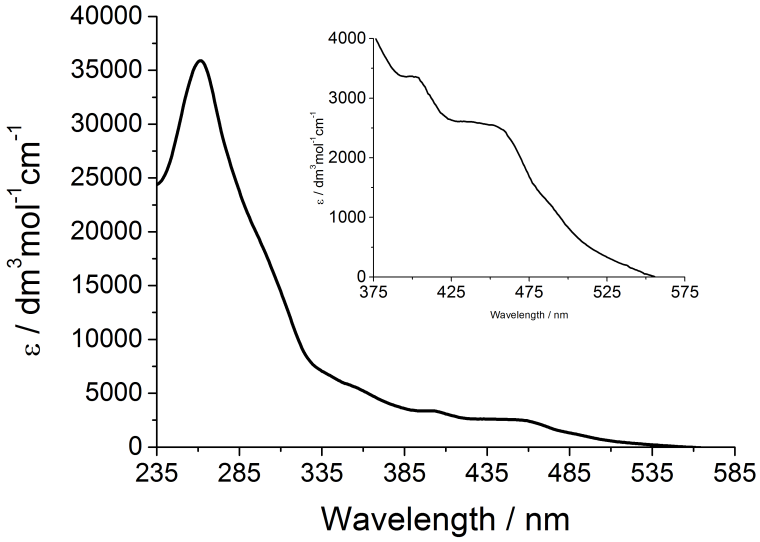

Fig. 6. UV-vis absorption spectrum of [Ir(ppy)$_2$(sq)] in CH_2Cl_2 (3.00×10^{-5} mol dm^{-3}).

3.5 Electrochemistry

The semiquinone complex exhibits three electrochemical events in CH_3CN over the investigated region of –2.70 to +1.35 V *versus* Fc/Fc^+ (Fig. 7). The quasi-reversible reduction centered at –0.61 V is attributed to the benzene-1,2-diolate/semiquinone redox couple. This value can be compared to those reported for analogous redox couples found in [Ir(2-(p-tolylpyridine))$_2$(DTBsq)], [Bu_4N][Ir(ppy)$_2$(TCC)], and

$[Bu_4N][Ir(ppy)_2(TBC)]$ (TBC = tetrabromobenzene-1,2-diolate) of –0.88, –0.19, and –0.18 V, respectively [21],[22] . A quasi-reversible oxidation assigned to the semiquinone/quinone couple was found at +0.20 V and is again found to be between those of $[Ir(2\text{-}(p\text{-tolylpyridine}))_2(DTBsq)]$ and the perhalogenated benzene-1,2-diolate complexes $[Bu_4N][Ir(ppy)_2(TCC)]$ and $[Bu_4N][Ir(ppy)_2(TBC)]$, reported as +0.08, +0.54, and +0.53 V, respectively. Finally, a quasi-reversible oxidation that is believed to arise from the oxidation of Ir(III) to Ir(IV) was observed at +1.02 V. A similar value of +0.90 V was measured for the same redox couple in $[Ir(2\text{-}(p\text{-tolylpyridine}))_2(DTBsq)]$ [22].

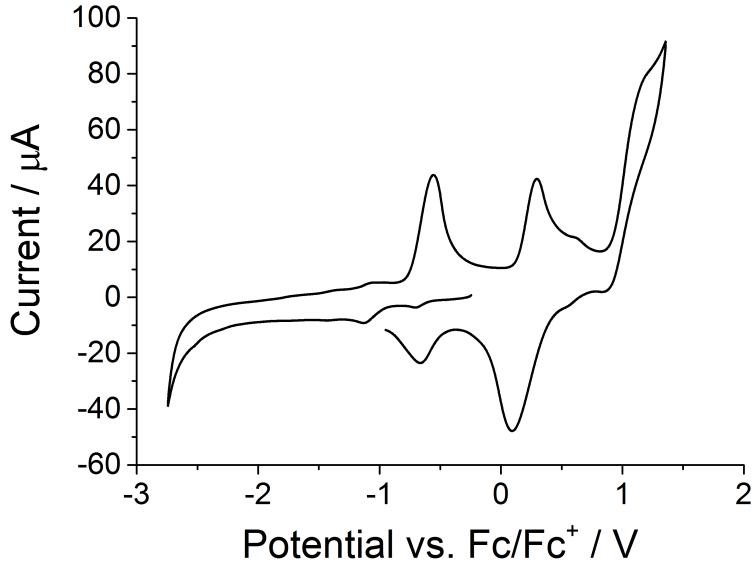

Fig. 7 Cyclic voltammogram of $[Ir(ppy)_2(sq)]$ in degassed CH_3CN with respect to Fc/Fc^+; scan rate = 0.1 V s^{-1}.

3.6 Spectroelectrochemistry

Given the fact that the iridium(III) complex containing the catecholate ligand readily converts from a reduced form to a more stable oxidized form with a notable change in color, $[Ir(ppy)_2(sq)]$ was investigated by spectroelectrochemistry. A dilute CH_2Cl_2 solution of $[Ir(ppy)_2(sq)]$ containing $[^nBu_4N][PF_6]$ as supporting electrolyte was added to an optically transparent thin-layer electrochemical

(OTTLE) cell and the potential scanned from –0.4 to +0.9 V and from –0.3 to –2.1 V relative to Fc/Fc^+, recording a UV-vis spectrum every 100 mV. In the forward direction, the absorption maximum at 261 nm diminishes to ~40% of its initial extinction coefficient at the highest applied potential of +0.9 V (Fig. 8a). The shoulder at 297 nm is diminished along with the maximum at 261 nm starting at roughly the same potential, but loses only 40% of its initial intensity. Both of these absorptions, which are attributed to ligand-centered $\pi^*\leftarrow\pi$ transitions, appear to be reversible and recover completely during the return scan (Fig. 8b). The relatively weak absorption at 453 nm assigned to an MLCT transition begins to lose intensity at +0.2 V, coinciding with the signal observed for the semiquinone/quinone redox couple in the standard cyclic voltammetry measurement. A new absorption at 663 nm also begins to grow in at this potential. The MLCT band at 453 regains most of its intensity returning to the starting potential while the new absorption at 663 nm is lost completely. When scanning to greater positive potentials (~1.5 V versus Fc/Fc^+), the spectra appear much less reversible with many of the absorptions losing a majority of their intensities. This corresponds with the irreversible oxidation of the Ir(III) to Ir(IV) and may indicate the partial decomposition of the complex.

Fewer changes in the absorption spectrum are observed when performing the reduction spectroelectrochemistry, whereby the neutral semiquinone is converted to an anionic benzene-1,2-diolate complex (Fig. 9). A slight increase in absorbance for the maximum at 261 nm is observed at the most negative potentials and two new broad absorptions grow in at 394 and 478 nm beginning at a potential of ~–1.3 V. Tetra(*n*-butyl)ammonium salts of the complexes $[Ir(ppy)_2(TCC)]^-$ and $[Ir(ppy)_2(TBC)]^-$ display similar absorptions in CH_3CN solutions with a peak maxima ~260 nm with weaker absorptions at ~290, ~370, and ~450 nm attributed to $\pi^*\leftarrow\pi$ and MLCT transitions.

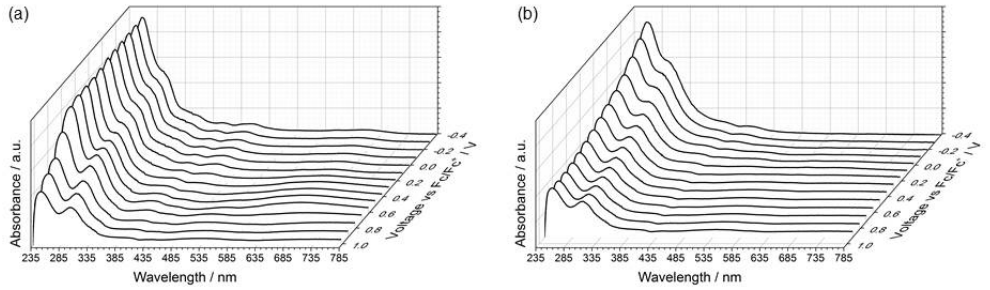

Fig. 8 Spectroelectrochemistry of $[Ir(ppy)_2(sq)]$ scanning to positive potentials in the (a) forward and (b) reverse direction. Corresponding 2D overlay plots are shown in Fig. S1.

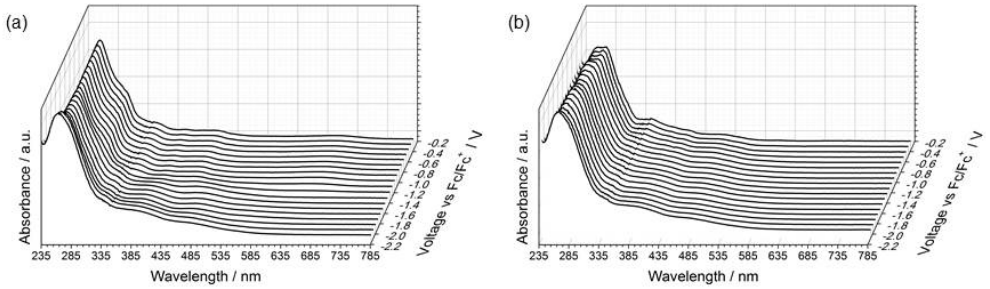

Fig. 9 Spectroelectrochemistry of $[Ir(ppy)_2(sq)]$ scanning to negative potentials in the (a) forward and (b) reverse direction. Corresponding 2D overlay plots are shown in Fig. S2.

4. Conclusions

In conclusion, the new anionic complex $[Ir(ppy)_2(cat)]^-$ was synthesized and isolated as the $[Me_4N]^+$ salt, and its structure confirmed by single crystal X-ray diffraction. Further characterization was not possible given the fast oxidation of the reduced benzene-1,2-diolate form of the complex to the *o*-semiquinone. Investigation of $[Ir(ppy)_2(sq)]$ using EPR spectroscopy indicates that the electron resides mainly on the bound dioxolene ligand in the paramagnetic complex with a g value close to that of a free electron and other related complexes. This is consistent with ^1H NMR spectroscopic data. No EPR signal was observed for the diamagnetic anionic complex, however, condensed oxygen in the sample caused its oxidation when cooling to 100 K for low temperature measurements. Evidence of both

semiquinone/catechol and semiquinone/quinone redox couples were observed in cyclic voltammetry. A significant change in the absorption properties of the complex was also observed using spectroelectrochemistry when oxidizing the semiquinone complex to its quinone form. Conversely, the absorption spectrum was only minimally affected when reducing the compound to its catecholate form.

Appendix 1 Supplementary data

Crystallographic data for all the complexes have been deposited with the CCDC (Cambridge Crystallographic Data Centre, 12 Union Road, Cambridge CB2 1EZ, UK; fax +44 1223 336 033; e-mail: deposit@ccdc.cam.ac.uk or www: http://www.ccdc.cam.ac.uk) and may be obtained free of charge on quoting the deposition numbers CCDC 1423808. Figs. S1 and S2: Spectroelectrochemistry of $[Ir(ppy)_2(sq)]$.

Acknowledgements

We thank the Swiss National Science Foundation, the European Research Council (Advanced Grant 267816 LiLo) and the University of Basel for financial support. The Swiss National Science Foundation is also thanked under R'equip SNF (project 206021_139133) for finance towards the EPR instrument.

References

[1] R.D. Costa, E. Ortí, H.J. Bolink, F. Monti, G. Accorsi, N. Armaroli, Angew. Chem., Int. Ed. 51 (2012) 8178.

[2] S.B. Meier, D. Tordera, A. Pertegás, C. Roldán-Carmona, E. Ortí, H.J. Bolink, Mater. Today 17 (2014) 217.

[3] E. Baranoff, J.-H. Yum, M. Graetzel, M.K. Nazeeruddin, J. Organomet. Chem. (2009) 2661.

[4] Y. Chi, P.-T. Chou, Chem. Soc. Rev. 39 (2010) 638.

[5] H. Xu, R. Chen, Q. Sun, W. Lai, Q. Su, W. Huang, X. Liu, Chem. Soc. Rev. 43 (2014) 3259.

[6] C. Fan, C. Yang, Chem. Soc. Rev. 43 (2014) 6439.

[7] E. Baranoff, B.F.E. Curchod, Dalton Trans. 44 (2015) 8318.

[8] T. Hu, L. He, L. Duan, Y. Qiu, J. Mater. Chem. 22 (2012) 4206.

[9] D. Tordera, A.M. Bünzli, A. Pertegás, J.M. Junquera-Hernández, E.C. Constable, J.A. Zampese, C.E. Housecroft, E. Ortí, H.J. Bolink, Chem. Eur. J. 19 (2013) 8597.

[10] A.M. Bünzli, H.J. Bolink, E.C. Constable, C.E. Housecroft, J.M. Junquera-Hernández, M. Neuburger, E. Ortí, A. Pertegás, J.J. Serrano-Pérez, D. Tordera, J.A. Zampese, Dalton Trans. 43 (2014) 738.

[11] E.C. Constable, C.E. Housecroft, G.E. Schneider, J.A. Zampese, H.J. Bolink, A. Pertegás, C. Roldan-Carmona, Dalton Trans. 43 (2014) 4653.

[12] D.P. Ris, G.E. Schneider, C.D. Ertl, E. Kohler, T. Müntener, M. Neuburger, E.C. Constable, C.E. Housecroft, J. Organomet. Chem. (2015) doi: 10.1016/ j.jorganchem.2015.08.021.

[13] I. González, P. Dreyse, D. Cortés-Arriagada, M. Sundararajan, C. Morgado, I. Brito, C. Roldán-Carmona, H.J. Bolink, B. Loeb, Dalton Trans. 44 (2015) 14771.

[14] C.D. Sunesh, G. Mathai, Y. Choe, ACS Appl. Mater. Interfaces 6 (2014) 17416.

[15] M. Mydlak, C. Bizzarri, D. Hartmann, W. Sarfert, G. Schmid, L. De Cola, Adv. Funct. Mater. 20 (2010) 1812.

[16] H.-F. Chen, C. Wu, M.-C. Kuo, M.E. Thompson, K.-T. Wong, J. Mater. Chem. 22 (2012) 9556.

[17] D. Di Censo, S. Fantacci, F. De Angelis, C. Klein, N. Evans, K. Kalyanasundaram, H.J. Bolink, M. Grätzel, M.K. Nazeeruddin, Inorg. Chem. 47 (2008) 980.

[18] F. Dumur, Y. Yuskevitch, G. Wantz, C.R. Mayer, D. Bertin, D. Gigmes, Synth. Met. 177 (2013) 100.

[19] F. Dumur, G. Nasr, G. Wantz, C.R. Mayer, E. Dumas, A. Guerlin, F. Miomandre, G. Clavier, D. Bertin, D. Gigmes, Org. Electron. 12 (2011) 1683.

[20] M.K. Nazeeruddin, R. Humphry-Baker, D. Berner, S. Rivier, L. Zuppiroli, M. Graetzel, J. Am. Chem. Soc. 125 (2003) 8790.

[21] E.I. Szerb, A. Ionescu, N. Godbert, Y.J. Yadav, A.M. Talarico, M. Ghedini, Inorg. Chem. Comm. 37 (2013) 80.

[22] B. Hirani, J. Li, P.I. Djurovich, M. Yousufuddin, J. Oxgaard, P. Persson, S.R. Wilson, R. Bau, W.A. Goddard, M.E. Thompson, Inorg. Chem. 46 (2007) 3865.

[23] M.D. Stallings, M.M. Morrison, D.T. Sawyer, Inorg. Chem. 20 (1981) 2655.

[24] S. Sprouse, K.A. King, P.J. Spellane, R.J. Watts, J. Am. Chem. Soc. 106 (1984) 6647.

[25] Bruker Analytical X-ray Systems Inc., (2006) APEX2 Version 2 User Manual M86 E01078 Madison WI.

[26] A. Altomare, G. Cascarano, C. Giacovazzo, A. Guagliardi, M.C. Burla, G. Polidori, M. Camalli, J. Appl. Crystallogr. 27 (1994) 435.

[27] G.M. Sheldrick, Acta Crystallogr. Sect. A 64 (2008) 112.

[28] I.J. Bruno, J.C. Cole, P.R. Edgington, C.F. Macrae, J. Pearson, R. Taylor, Acta Crystallogr. Sect. B B58 (2002) 389.

[29] C.F. Macrae, I.J. Bruno, J.A. Chisholm, P.R. Edgington, P. McCabe, E. Pidcock, L. Rodriguez-Monge, R. Taylor, J. Van De Streek, P.A. Wood, J. Appl. Crystallogr. 41 (2008) 466.

[30] P. Barbaro, C. Bianchini, K. Linn, C. Mealli, A. Meli, F. Vizza, F. Laschi, P. Zanello, Inorg. Chim. Acta 198-200 (1992) 31.

[31] P.A. Wicklund, L.S. Beckmann, D.G. Brown, Inorg. Chem. 15 (1976) 1996.